COBEM 2023 27TH INTERNATIONAL CONGRESS OF MECHANICAL ENGENEERING

ABCM Brazilian Society of Mechanical Sciences and Engineering
27th ABCM International Congress of Mechanical Engineering
December 04-08, 2023, Florianópolis-SC, Brazil

COB-2023-1251

SHM based on the Electromechanical Impedance Technique with Temperature Variations: Theoretical and Experimental Approach

Lorena Lopes Dias
lorena.dias@unesp.br
Douglas D. Bueno
douglas.bueno@unesp.br
Camila G. Gonsalez-Bueno
camila.gg.bueno@unesp.br

Group of Intelligent Materials and Systems (GMSINT), Advanced Systems Laboratory (LSA), School of Engeneering (FEIS), Sao Paulo State University (UNESP), Brasil Avenue, 56, Ilha Solteira, SP, 15.385-000, Brazil

Abstract. *To ensure that structures operate within their safety standards and have high performance in operation, an area known as Structural Health Monitoring (SHM) was created. This comprises a set of techniques capable of detecting damage at early stages. In particular, the Electromechanical Impedance (EMI) technique has attracted attention due to its promising results. In general, this technique is most often studied when based on experimental signals, which may limit its physical understanding. However, in recent years, there has been an effort by the scientific community to broaden the understanding of the EMI technique by considering numerical-computational simulations. In this context, the present work investigates the feasibility of an analytical model present in the literature to determine the electromechanical impedance curves of an Euler-Bernoulli beam at different temperatures, since the sensitivity of this technique to temperature variations can lead to incorrect diagnoses in SHM. In this work, a wider temperature range was investigated than the one used in reference literature. A numerical and experimental approach was employed. The theoretical and experimental results obtained for different temperatures are in close agreement with each other, especially regarding the position of EMI peaks.*

Keywords: *Structural Health Monitoring, Electromechanical Impedance, Temperature, Analytical Model, Experimental Data.*

1. INTRODUCTION

During the service life and operating time of the different engineering structures, they are subjected to various comprehensive stresses and factors responsible for the accumulation of damage and deterioration of their performances (Han *et al.*, 2021). In view of this, different numerical and experimental studies are carried out for developing new techniques to evaluate and monitor structural systems, aiming to identify any changes in material and geometric properties that could be an indication of possible damage (Worden and Dulieu-Barton, 2004; Farrar *et al.*, 2005). This field is known as Structural Health Monitoring (SHM), mainly focused on detecting damage in its early stages.

Among the methods employed in SHM, the Electromechanical Impedance (EMI) technique stands out due to its ability to detect incipient damage using non-intrusive piezoelectric transducers and to be a potential low-cost application (Yang *et al.*, 2008; Selva *et al.*, 2013). It was first suggested by Liang *et al.* (1993) and currently there are promising results known in the literature, mainly involving real-time signal processing. This technique typically comprises the use of piezoelectric transducers, especially ceramics PZT (Leads Zirconate Titanate), that act as both actuator and sensor, i.e., it excites the monitored structure and measures its response (Wang *et al.*, 2014). Its approach basically consists on measuring EMI for the non-damage condition, known as baseline signal, and then, this data is compared with other EMI signals obtained for unknown structural conditions (Sun and Rogers, 1995; Gyuhae Park and Inman, 2003; Bhalla and Soh, 2004).

There are many works investigating EMI-based techniques, and most of them involve post-processing experimental data (Divsholi and Yang, 2012; Luo *et al.*, 2013; Ai *et al.*, 2014; Campeiro *et al.*, 2018). However, in recent years, there has been an effort by the scientific community to broaden the understanding of EMI technique by considering numerical-computational simulations, which allow a variety of parameters and damage scenarios to be simulated. This enables response trends and parameter dependencies to be analyzed more explicitly and, hence, a better understanding of the technique. Wang *et al.* (2015) implement an electromechanical impedance analysis of a piezoelectric smart beam with a crack, simulated using spring models. Spectral element method (SEM) is used to analyze the EMI response of the piezoelectric smart beam for different crack depths. Similar work is presented by Zhang *et al.* (2011), considering an analytical model for a Timoshenko beam. Yan *et al.* (2011) develop an analytical model of a cracked functionally graded beam with attached PZTs, in which they describe the bonding imperfection between the piezoelectric transducers and the

structure by means of a viscoelastic law. Hamzeloo *et al.* (2020) introduce a new theoretical model for damage detection of L-shaped beams, in which the electromechanical impedance at each point of the structure is determined by calculating the dynamic stiffness of structures. Comprehensive work is presented by Sepehry *et al.* (2010), Sepehry *et al.* (2014) and Sepehry *et al.* (2017). The authors detail different formulations, for beams and plates, showing interesting correlation between simulations and experimental tests, considering the influence of ambient temperature on damage detection.

Despite several studies demonstrating the feasibility of applying EMI technique, practical problems have prevented its efficient and reliable use in real structures, with temperature effects considered one of the most critical and challenging (Baptista *et al.*, 2014). Electromechanical impedance signals are directly affected by changes in properties of structure and piezoelectric transducers. Consequently, temperature acts as a key factor for the performance of an SHM system via impedance, since it is responsible for altering materials properties. In view of this, several researchers investigate the influences of temperature on EMI technique. In general, these researches state that temperature variations introduce changes in frequency and magnitude, as well as peak smoothing, of the EMI curves (Sepehry *et al.*, 2010; Baptista *et al.*, 2012; Xu *et al.*, 2016; Abbas *et al.*, 2021), which can lead to incorrect diagnosis of the integrity of the monitored structure.

In this context, the present work comprises the implementation and investigation of the analytical model developed by Sepehry *et al.* (2010) for obtaining the Electromechanical Impedance curves of an Euler-Bernoulli beam. The numerical study was experimentally validated for the temperature range from 24°C to 70°C, which is wider than the one analyzed by Sepehry *et al.* (2010) (25°C to 50°C). The theoretical and experimental results obtained for different temperatures are in close agreement with each other, especially regarding the position of EMI peaks.

2. METHODOLOGY

This section presents the description of the methods and procedures employed in this work. Initially, a brief explanation of the Electromechanical Impedance is presented, Subsection 2.1. Next, the numerical approach used to calculate the theoretical EMI is addressed in Subsection 2.2. Finally, the experimental approach employed is described in Subsection 2.3.

2.1 Electromechanical Impedance

Electromechanical Impedance technique consists of using one or more piezoelectric transducers as sensor(s) and actuator(s). These devices are responsible for the coupling between structure's mechanical impedance and PZT's electrical impedance, from which the monitoring of structure is carried out (Na and Baek, 2018).

The admittance $Y_{em}(\omega)$, represented in Eq. (1), was introduced by Liang *et al.* (1993); and its inverse corresponds to the electromechanical impedance $Z_{em}(\omega)$. This equation shows how the structure's mechanical impedance, $Z(\omega)$, and the piezoelectric transducer's mechanical impedance , $Z_A(\omega)$, relate to each other to define the electromechanical impedance of the system.

$$Y_{em}(\omega) = j\omega \frac{b_p L_p}{h_p} \left[\bar{\epsilon}_{33}^{T} - \frac{Z(\omega)}{Z_A(\omega) + Z(\omega)} d_{31} \bar{Y}_{11}^{E} \right] \tag{1}$$

where L_p, b_p and h_p are the length, width and thickness of the PZT, respectively. $\bar{\epsilon}_{33}^{T}$ is the dielectric constant of the PZT in the 3-3 direction (z) under a constant voltage, d_{31} is the piezoelectric constant, $\bar{Y}_{11}^{E}$ is the complex elastic modulus of the PZT in the 1-1 direction (x) under a constant electric field; and $j = \sqrt{-1}$ is the pure imaginary number.

2.2 Numerical Approach

The analytical model is developed by Sepehry *et al.* (2010) and used to calculate the electromechanical impedance of a beam with attached PZT, as shown in Fig. 1. First, the authors determine the kinetic and strain energies of both components of the mechanical system (beam and PZT) separately and, then, combined. Next, the Lagrange Equation for the case without external forces is applied, obtaining the system dynamic given by

$$\mathbf{M}\ddot{\mathbf{q}}(t) + \mathbf{K}\mathbf{q}(t) = \mathbf{N}E_3 \tag{2}$$

where $\mathbf{M}$ is the total mass matrix obtained by summing the matrices of the beam and the PZT, and similarly, $\mathbf{K}$ is the total stiffness matrix; $\mathbf{q}(t)$ is the modal displacement vector, $\mathbf{N}$ is the moment vector created by PZT and E_3 is the electric field.

The authors consider the masses and stiffnesses of the beam and PZT written in terms of the modal shape functions $\psi_i(x)$, where i is the ith mode. The mass matrices of the beam, $\mathbf{M}_b$, and of the piezoelectric transducer, $\mathbf{M}_p$, are such that each element in the ith row and jth column is given respectively by

$$m_b^{(i,j)} = \int_0^{L_b} \bar{\rho}_b A_b \psi_i(x) \psi_j(x) dx \qquad m_p^{(i,j)} = \int_{x_1}^{x_2} \rho_p A_p \psi_i(x) \psi_j(x) dx \tag{3}$$

in which the subscript b denotes the beam; and p denotes the PZT, positioned between the coordinates x_1 and x_2, such that $(x_2 - x_1) = L_p$ (see Fig. 1). $\bar{\rho}_b$ and ρ_p are, respectively, the densities of the beam and the PZT. A_b and A_p are

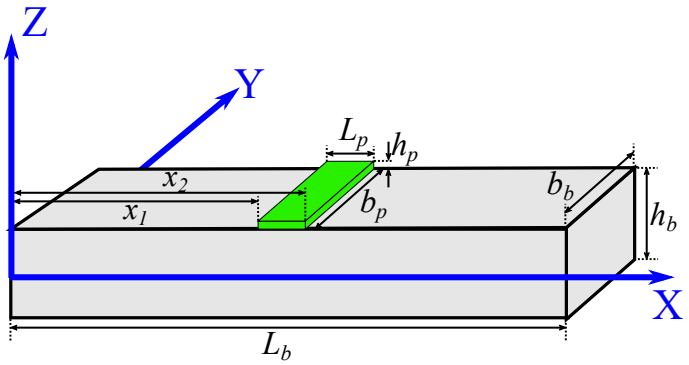

Figure 1. Schematic of a beam with attached PZT.

the respective cross section areas and L_b is the length of the beam. Furthermore, the elements of the respective stiffness matrices are determined by

$$k_b^{(i,j)} = \int_0^{L_b} \bar{E}_b I_b \psi_i''(x)\psi_j''(x)dx \qquad k_p^{(i,j)} = \int_{x_1}^{x_2} I_1 \psi_i''(x)\psi_j''(x)dx \tag{4}$$

where $\bar{E}_b$ is the Young's modulus of the beam, I_b is the second moment of area of the beam and I_1 is the constant given by: $I_1 = cb_b \frac{z}{3}\Big|_{h_b/2}^{h_b/2+h_p}$, such that c is the inverse of the mechanical compliance S_{11}^E for zero electric field, and b_b and h_b are the width and thickness of the beam, respectively. The superscript $(\,)''$ indicates the second derivative, with respect to x. The subscript $\bar{(\,)}$ indicates the temperature dependence. The momentum vector $\mathbf{N}$ is such that its i-th element is given by $N_p^{(i)} = -\int_{x_1}^{x_2} I_2 \psi_i''(x)dx$, where $I_2 = db_p z^2\Big|_{h_b/2}^{h_b/2+h_p}$ and $d = \dfrac{\bar{d}_{31}}{S_{11}^E}$.

Then, the authors rewrite the vector $\mathbf{q}(t)$ as a multiplication between the generalized coordinates of the system $\mathbf{g}(t)$ and the matrix of eigenvectors of the system for zero electric field $\mathbf{\Phi}$, such that $\mathbf{M}_{gg}\ddot{\mathbf{g}}(t) + \mathbf{K}_{gg}\mathbf{g}(t) = \mathbf{\Phi}^T\mathbf{N}E_3$, where $\mathbf{M}_{gg} = \mathbf{\Phi}^T\mathbf{M}\mathbf{\Phi}$ and $\mathbf{K}_{gg} = \mathbf{\Phi}^T\mathbf{K}\mathbf{\Phi}$. The structural damping matrix $\mathbf{C}_{gg}$ is introduced using the Rayleigh proportional damping as:

$$\mathbf{C}_{gg} = \alpha\mathbf{M}_{gg} + \beta\mathbf{K}_{gg} \tag{5}$$

where α and β are arbitrary constant coefficients. These are determined aiming to transmit appropriate damping values to the system under investigation (Hall, 2006).

Sepehry *et al.* (2010), then, assume that the electric field E_3 is uniform over the PZT, and can be written in terms of the electric voltage V_3, such that $E_3 = V_3/h_p$. Furthermore, they consider a harmonic voltage $V_3 = V_0 e^{j\omega t}$ and $\mathbf{g}(t) = g_0 e^{j\omega t}$. Thus, the electromechanical impedance Z_{em} of the system is given by

$$Z_{em}(\omega) = \left\{ j\omega \left[-db_p \left(\frac{h_b}{2}\right) \Psi'(x)|_{x_1}^{x_2} \mathbf{\Phi} \left(-\omega^2\mathbf{M}_{gg} + \mathbf{C}_{gg}j\omega + \mathbf{K}_{gg}\right)\mathbf{N}_g + \frac{e_p b_p L_p}{h_p} \right] \right\}^{-1} \tag{6}$$

where $\mathbf{N}_g = \mathbf{\Phi}^T\mathbf{N}/h_p$, $e_p = \bar{\epsilon}_{33}^T - \dfrac{\bar{d}_{31}^2}{S_{11}^E}$ and $\Psi(x) = [\psi_1(x) \;\; \psi_2(x) \;\; \ldots \;\; \psi_n(x)]$ is the modal shape matrix, obtained for n modes.

2.2.1 Rayleigh Damping

Damping is the phenomenon responsible for the dissipation of mechanical energy in engineering systems. Consequently, the attenuation of vibration and the dynamic response of structures are governed by this phenomenon (Liu and Gorman, 1995). Despite its crucial role in describing the behavior of mechanical systems, understanding and characterizing this property can still be challenging, especially for more complex structures. In such cases, damping is often directly introduced into the dynamic equation, with Rayleigh damping being a widely utilized approach for modeling structural damping (Han *et al.*, 2021). This is determined through a linear combination of mass and stiffness, as demonstrated in Eq. (5).

In this study, the *fminsearch* command of the Matlab® software was employed to determine the Rayleigh damping coefficients α and β. This command utilizes the Nelder-Mead numerical method to locate the minimum of a multivariate function, denoted as fun. In this context, fun was defined as the absolute difference between the corresponding electromechanical impedances at the highest experimentally and theoretically measured peak, obtained at 24°C, as represented in

Eq. (7). In other words, the computational command repeatedly recalculated the theoretical electromechanical impedance until the function fun reached its minimum value.

$$fun = |max(Z_{exp}(\omega_i)) - max(Z_{theo}(\omega_i))|, \quad i = f_{min}, f_{min}+1, ..., f_{max} \tag{7}$$

where $max(\ )$ denotes the maximum value, Z_{exp} and Z_{theo} represent the experimental and theoretical electromechanical impedances, respectively, and f_{min} and f_{max} correspond to the minimum and maximum frequencies of the analyzed frequency interval, which are equivalent to 15 kHz and 30 kHz, respectively, as will be clarified later. The calculated values are presented in Tab. 5.

2.2.2 Modal Shape Functions for High Frequencies

Engineering structures, when excited at their natural frequencies, vibrate or deform in particular ways known as modal shapes. In other words, the vibration modes portray the way the structure vibrates. Under typical operating conditions, a structure will vibrate in a complex combination of all mode shapes (Gonçalves *et al.*, 2007; Gomes and Giovani, 2022). In this work, the exact expression of the modal shape function obtained by Gonçalves *et al.* (2018) for an Euler-Bernoulli beam in the free-free condition was used, which is presented in Eq. (8). The wavenumbers k_n related to the natural frequencies of the beam are presented in Tab. 1.

$$\psi_n(x) = \left[\frac{-e^{(k_n(x-2L_b))} + [cos(k_nL_b) - sen(k_nL_b)]e^{(k_n(x-L_b))}}{1 - e^{(-2k_nL_b)} - 2sen(k_nL_b)e^{(-k_nL_b)}}\right] + \frac{1}{2}e^{(-k_nx)}(1+\eta_n) + cos(k_nx) - \eta_n sen(k_nx) \tag{8}$$

where

$$\eta_n = \frac{1 + e^{(-2k_nL_b)} - 2e^{(-k_nL_b)}cos(k_nL_b)}{1 - e^{(-2k_nL_b)} - 2e^{(-k_nL_b)}sen(k_nL_b)} \tag{9}$$

Table 1. Wavenumbers k_n.

n	k_nL_b
1	4.73004
2	7.85320
3	10.9956
4	13.3518
5	16.4934
$n > 5$	$\frac{(2n+1)\pi}{2}$

The formula described in Eq. (8) must be used when the Euler-Bernoulli beam theory is valid, that is, when the wavelength of a flexural wave is approximately ten times greater than the beam thickness (Gebhart, 1969; Gonçalves *et al.*, 2018). This equation remains applicable across a broad frequency spectrum, including high frequencies, as long as it falls within the validity of the Euler-Bernoulli beam theory, regardless of the number of modes needed.

From the k_nL_b expression presented in Tab. 1 and the flexural wavenumber of an Euler-Bernoulli beam given by $k = (\rho_bA_b/E_bI_b)^{1/4}\omega^{1/2}$, it is possible to determine the number of modes required for the analysis of the beam that represent the entire frequency range investigated. In this study, 35 structural modes were used for the numerical simulations, since the maximum frequency analyzed corresponds to 30 kHz, as will be clarified later.

2.2.3 Theoretical Effects of Temperature Variations

Materials properties vary with temperature. In the electromechanical impedance technique, temperature affects the properties of the piezoelectric transducer and the structure, which can lead to incorrect diagnoses when monitoring the structural integrity if an unknown structural condition is obtained in a temperature T_{j+1} and then compared with a baseline condition obtained in a different temperature T_j. In view of this, the behavior of the electromechanical impedance curves is analyzed for a temperature range from 24°C to 70°C, which is slightly wider than the one studied by Sepehry *et al.* (2010) (25°C to 50°C).

In this work, the PSI-5H4E piezoelectric transducer manufactured by *Piezo Systems*® was used to monitor the structure integrity. Information on its properties was obtained from the technical document provided by the piezoelectric ceramic manufacturer. Table 4 presents the properties of this PZT at the reference temperature, which corresponds to 24°C. In addition, its properties were investigated at nine other different temperatures: 30°C, 35°C, 40°C, 45°C, 50°C, 55°C, 60°C,

65°C and 70°C. These data were extracted from the temperature-dependent property curves found in the piezoelectric ceramic datasheet. Using these data, an equation was formulated to describe the behavior of the PZT properties in response to temperature, covering the temperature range of interest from 24°C to 70°C. Table 2 presents the values of the dielectric constant $\bar{\varepsilon}_{33}^{T}$ and the piezoelectric constant $\bar{d}_{31}$ as a function of temperature, along with the corresponding equations that describe these variations.

Table 2. PSI-5H4E piezoelectric transducer properties as a function of temperature.

Property	**30°C**	**35°C**	**40°C**	**45°C**	**50°C**	**55°C**	**60°C**	**65°C**	**70°C**
$\bar{d}_{31}$ [10^{-12} m/V]	-334.06	-339.79	-345.52	-351.25	-356.98	-362.71	-368.44	-374.17	-379.90
$\bar{\varepsilon}_{33}^{T}$ [10^{-8} F/m]	3.388	3.520	3.665	3.824	3.996	4.182	4.381	4.594	4.820

$\bar{d}_{31}(°C) = -1.1459 \times T - 299.6837$ e $\bar{\varepsilon}_{33}^{T}(°C) = 0.3040 \times T^2 + 10.0408 \times T + 3.2537 \times 10^3$.

In this study, a beam made of 6063-T5 aluminum alloy was investigated. The Aluminum Design Manual (ADM) (Aluminum Association - AA, 2010) was utilized to extract the Young's modulus $\bar{E}_b$ values at different temperatures and to formulate an equation to describe these variations. The manual provides tabular values of this property at elevated temperatures, from which linear interpolation was performed to derive an equation that covered the temperature range of interest, i.e., from 24°C to 70°C. The same procedure was adopted to obtain the material density $\bar{\rho}_b$ values, with the distinction that the reference source used for this purpose was authored by Meseguer *et al.* (2019). The values of the Young's modulus $\bar{E}_b$ and density $\bar{\rho}_b$ as a function of temperature, along with the equations describing these variations, are presented in Tab. 3. This table provides data for the nine temperatures (30°C, 35°C, 40°C, 45°C, 50°C, 55°C, 60°C, 65°C and 70°) different from the reference temperature (24°C), which is documented in Tab. 5.

Table 3. Properties of the 6063-T5 aluminum alloy as a function of temperature.

Property	**30°C**	**35°C**	**40°C**	**45°C**	**50°C**	**55°C**	**60°C**	**65°C**	**70°C**
$\bar{E}_b$ [GPa]	68.783	68.601	68.419	68.238	68.056	67.875	67.693	67.511	67.330
$\bar{\rho}_b$ [kg/m^3]	2679	2678	2677	2676	2675	2674	2673	2672	2671

$\bar{E}_b(°C) = -3.6316 \times 10^7 \times T + 6.9872 \times 10^{10}$ e $\bar{\rho}_b(°C) = -0.2 \times T + 2.6850 \times 10^3$.

2.3 Experimental Approach

The experiment consisted of collecting electromechanical impedance signals from a 6063-T5 aluminum alloy beam containing a PSI-5H4E piezoelectric transducer from Piezo Systems® attached to its surface. Figure 2 shows a schematic of the experimental setup utilized. It was used a National Instruments® board, model NI-USB 6211 (16 bits); a computer containing the software with the impedance analyzer developed by Baptista and Filho (2009) in LabVIEW® environment; and a *protoboard* containing a resistance of 10 $k\Omega$, which acts as an auxiliary circuit whose function is to limit the voltage in the piezoelectric transducer, thus avoiding potential damage to this device. The data acquisition (DAQ) board is responsible for capturing the response signal and, simultaneously, transmitting the excitation signal to the piezoelectric transducer. The excitation signal is generated by the impedance analyzer, which also calculates the electromechanical impedance based on the response signal captured by the DAQ. This software includes procedures for adjusting the measurement system and the excitation signal according to the user's wishes.

The aluminum beam was placed inside a thermal chamber from the brand Thermotron® S-Series to simulate ambient temperature variations. This beam was positioned on a foam layer to simulated a free-free boundary condition. Geometric and material properties of the piezoelectric transducer and the beam at 24°C are presented in Tabs. 4 and 5, respectively.

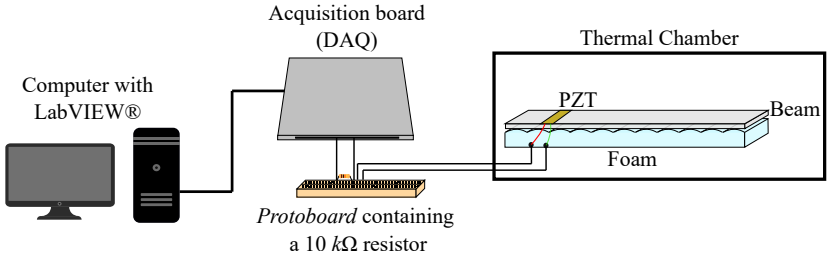

Figure 2. Experimental setup.

Table 4. Geometric and material properties of the PSI-5H4E piezoelectric transducer at 24°C.

Property	Symbol	Value
Length	L_p	13 mm
Width	b_p	12 mm
Thickness	h_p	0.2667 mm
Compliance	S_{11}^E	1.6129×10^{-11} Pa^{-1}
Density	ρ_p	7800 kg/m^3
Piezoelectric constant	$\bar{d}_{31}$	-327.18×10^{-12} m/V
Dielectric constant	$\bar{\varepsilon}_{33}^T$	$3.24783.3630\times10^{-8}$ F/m
Distance from the first PZT's end to the origin	x_1	81 mm
Distance from the second PZT's end to the origin	x_2	$x_1 + L_p$ = 94 mm

The signals were measured in a temperature range from 24°C to 70°C, which correspond to a large portion of the structures in operation. It was utilized a step of 5°C for the non-damage condition. In order to excite the structure, it was applied a sinusoidal frequency sweep with an amplitude of ±1 V in a frequency range of 1 Hz to 100 kHz, with a step size of 1 Hz. The signals were gauged only during heating. Thirty signals were collected for each temperature and a sampling rate of 250 kS/s was employed.

Table 5. Geometric and material properties of the 6063-T5 aluminum alloy beam at 24°C.

Property	Symbol	Value
Length	L_b	498 mm
Width	b_b	12 mm
Thickness	h_b	3 mm
Young's modulus	$\bar{E}_b$	69 GPa
Density	$\bar{\rho}_b$	2680 kg/m^3
Coefficient	α	0.0011
Coefficient	β	3.5315×10^{-8}

3. RESULTS AND DISCUSSION

In order to determine whether the analytical model is applicable at different temperatures, as well as to compare the theoretical and experimental curves for the 10 different temperatures selected (24°C, 30°C, 35°C, 40°C, 45°C, 50°C, 55°C, 60°C, 65°C and 70°C), a curve-by-curve comparison between these signals is presented below. All the numerical results were obtained using the algorithm implemented in the Python® software. In all cases, the electromechanical impedance curves were analyzed for the frequency range from 15 kHz to 30 kHz, which, through previous investigations, proved to be the most appropriate for the application of Sepehry *et al.* (2010) approach and with the best agreement with the experimental data used in this work.

The real part of the theoretical and experimental electromechanical impedance curves for the 10 different temperatures analyzed (24°C, 30°C, 35°C, 40°C, 45°C, 50°C, 55°C, 60°C, 65°C and 70°C) are shown in Figs. 3 to 7. The percentage errors between the peak frequencies of the experimental and theoretical signals are shown in Tab. 6.

Upon examining Figs. 3 to 7, it is possible to observe the presence of a peak with extremely low amplitude, located at approximately 24.2 kHz, in both the experimental and theoretical signals. These peaks were intentionally disregarded due to their low amplitude and difficulty of visualization. Furthermore, the experimental signals revealed the occurrence of some double peaks, i.e., peaks positioned very close to each other, which were not reflected in the theoretical analysis. For this reason, only the peak with the highest amplitude was considered for the comparative analysis. The presence of double peaks could be attributed to the discretization chosen for the acquisition of the experimental signals, which may have needed to be reduced.

In Figs. 3 to 7, the scales of numerical and experimental results are slightly different from each other, with the experimental curves showing a shift in amplitude that moves them away from the zero vertical axis. These divergences between the theoretical and experimental EMI signals may have several origins, such as the calibration of the measurement system, the parameters used in the theoretical system, non-ideal experiment boundary conditions, variables that influenced the experimental data that were not considered in the theoretical analysis, the input impedances caused by the conductor cables and the DAQ, as well as the influence of the auxiliary electrical circuit on the measured signal, which weren't compensated in the experimental curves or considered in the analytical model, among other reasons.

However, in all investigated scenarios, the numerical and experimental curves exhibited similar behaviors, especially

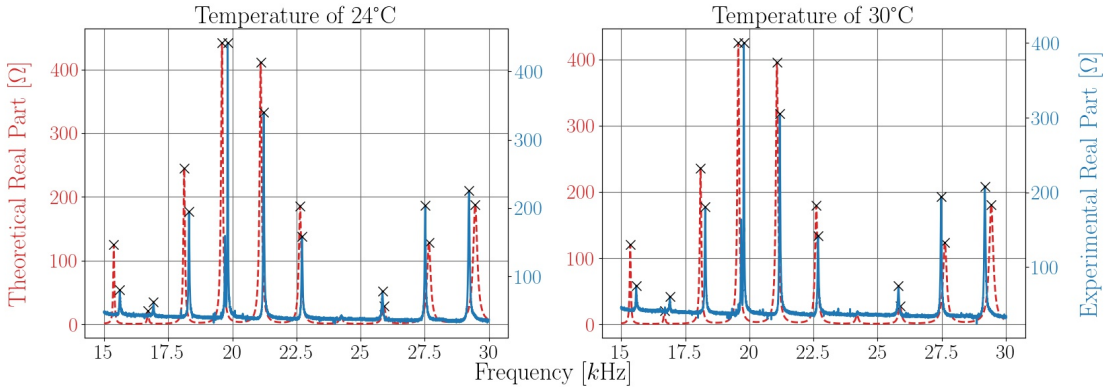

Figure 3. Real part of theoretical and experimental electromechanical impedance curves at 24°C and 30°C. Red dashed line represents the theoretical curve, blue solid line corresponds to the experimental curve and × indicates the peaks.

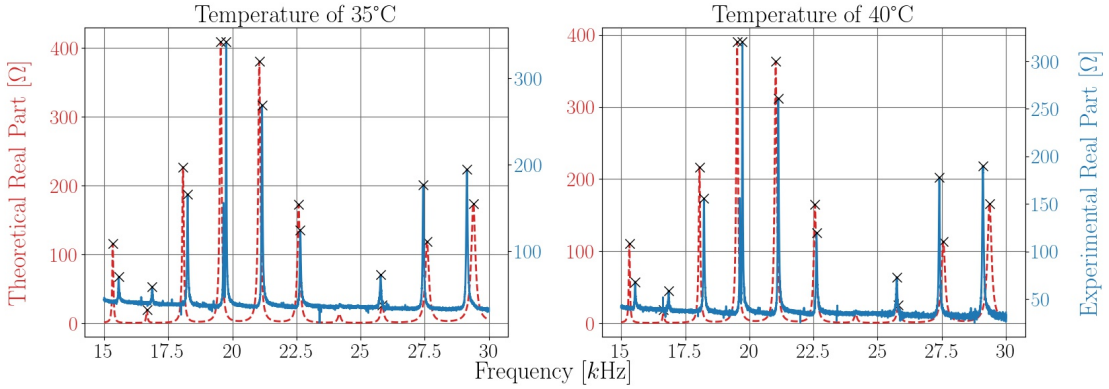

Figure 4. Real part of theoretical and experimental electromechanical impedance curves at 35°C and 40°C. Red dashed line represents the theoretical curve, blue solid line corresponds to the experimental curve and × indicates the peaks.

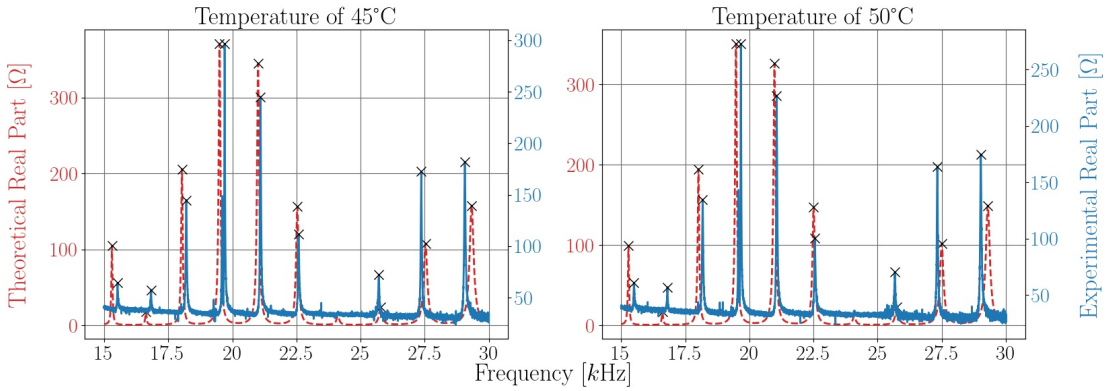

Figure 5. Real part of theoretical and experimental electromechanical impedance curves at 45°C and 50°C. Red dashed line represents the theoretical curve, blue solid line corresponds to the experimental curve and × indicates the peaks.

regarding the peaks location. The percentage errors consistently remained below 1.52% for all evaluated temperatures. In other words, even when considering different temperatures, the theory and experimental results showed a remarkable agreement regarding the peak positions, highlighting the effectiveness of the approach proposed by Sepehry *et al.* (2010). However, it is noticeable that as the temperature increases, the disparities between the axis scales of the two analyzed signals become more pronounced. This phenomenon occurs because the damping parameters (α and β) of the structure were selected based on data acquired at a temperature of 24°C, making them specifically tailored to that condition. Consequently, changes in damping values due to temperature fluctuations were not adequately incorporated into the theoretical model.

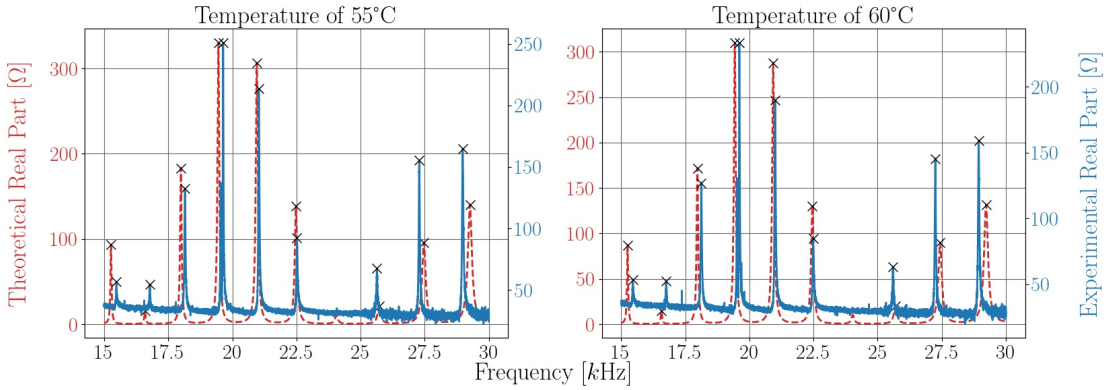

Figure 6. Real part of theoretical and experimental electromechanical impedance curves at 55°C and 60°C. Red dashed line represents the theoretical curve, blue solid line corresponds to the experimental curve and × indicates the peaks.

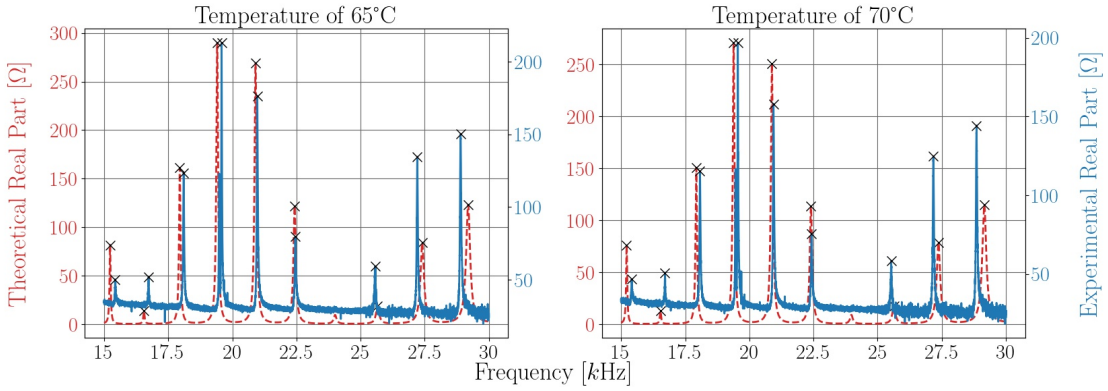

Figure 7. Real part of theoretical and experimental electromechanical impedance curves at 65°C and 70°C. Red dashed line represents the theoretical curve, blue solid line corresponds to the experimental curve and × indicates the peaks.

Table 6. Percentage error between experimental and theoretical peak frequencies for the 10 selected temperatures.

	Percentage errors [%]									
Temp. / **Peak**	**24°C**	**30°C**	**35°C**	**40°C**	**45°C**	**50°C**	**55°C**	**60°C**	**65°C**	**70°C**
1	1.51	1.49	1.48	1.44	1.40	1.37	1.35	1.32	1.26	1.28
2	1.28	1.25	1.23	1.21	1.18	1.15	1.13	1.10	1.07	1.05
3	1.03	0.99	0.99	0.96	0.93	0.91	0.88	0.84	0.82	0.80
4	1.13	1.10	1.08	1.04	1.01	0.98	0.94	0.90	0.87	0.83
5	0.55	0.52	0.51	0.48	0.45	0.41	0.38	0.36	0.32	0.30
6	0.33	0.30	0.29	0.27	0.23	0.20	0.17	0.16	0.11	0.11
7	0.21	0.23	0.24	0.27	0.28	0.31	0.33	0.37	0.37	0.41
8	0.52	0.54	0.55	0.58	0.60	0.61	0.66	0.69	0.71	0.72
9	0.83	0.85	0.86	0.89	0.92	0.93	0.98	0.99	1.02	1.05

4. CONCLUSIONS

This paper aimed to study, implement and investigate the analytical model developed by Sepehry *et al.* (2010) in order to contribute to the knowledge formation and greater understanding of the Electromechanical Impedance technique considering variations of the working temperature. The approach is evaluated on an aluminum beam with attached PZT in the non-damaged condition and was validated with experimental data.

A comparison between the numerical and experimental curves for the ten different temperatures (24°C, 30°C, 35°C, 40°C, 45°C, 50°C, 55°C, 60°C, 65°C and 70°C) was performed in order to investigate whether the numerical model is applicable in varying temperature conditions. Through this study, it was possible to verify that the two types of EMI signals showed similar behavior to each other in all temperatures, mainly with respect to the position of the peaks. However,

discrepancies in the axis scales were noted, which accentuated as the investigated temperature increased.

In conclusion, the analytical model developed by Sepehry *et al.* (2010) demonstrated a remarkable agreement with experimentally acquired data, despite the assumptions and idealizations considered in its formulation. This suggests that the model can be effectively employed to anticipate trends in electromechanical impedance curves in environments with temperature variations, especially concerning peak locations. However, it is important to emphasize that this model requires a prior understanding of structural damping or the acquisition of this knowledge through comparisons with experimental data, as done in this study. This may pose challenges in applying the model and compromise the primary advantage associated with using a theoretical model, which is the elimination of the need for any prior experimental information. Nevertheless, despite these considerations, the model has the capacity to extrapolate this data to different temperatures, thus reducing the necessity to conduct multiple experiments under various thermal conditions.

Lastly, it is important to emphasize the need for further research with the aim of evaluating the model's capability to replicate damages in various thermal conditions, thereby offering valuable insights into structural behavior in diverse environments and structural circumstances. Such an endeavor, in addition to contributing to the extension of the analytical model's applicability, holds the promise of enriching the understanding of complex structural interactions in diverse contexts.

5. ACKNOWLEDGEMENTS

The authors thank the São Paulo Research Foundation (FAPESP) under grant number 2021/12008-2; and Coordination for the Improvement of Higher Education Personnel (CAPES).

6. REFERENCES

Abbas, S., Li, F., Abbas, Z., Abbasi, T.U.R., Tu, X. and Pasha, R.A., 2021. "Experimental study of effect of temperature variations on the impedance signature of pzt sensors for fatigue crack detection". *Sound & Vibration*, Vol. 55, No. 1, pp. 1–18.

Ai, D., Zhu, H., Luo, H. and Yang, J., 2014. "An effective electromechanical impedance technique for steel structural health monitoring". *Construction and Building Materials*, Vol. 73, p. 97–104.

Aluminum Association - AA, 2010. *Aluminum Design Manual - ADM*. Washington, DC, 9th edition.

Baptista, F.G., Budoya, D.E., De Almeida, V.A.D. and Ulson, J.A.C., 2014. "An experimental study on the effect of temperature on piezoelectric sensors for impedancebased structural health monitoring". *Sensors 14*, pp. 1208–1227.

Baptista, F.G. and Filho, J.V., 2009. "A new impedance measurement system for pzt based structural health monitoring". *IEEE Transaction on Instrumentation and Measurement*, Vol. 58, No. 10, pp. 3602–3608.

Baptista, F.G., Filho, J.V. and Inman, D.J., 2012. "Real-time multi-sensors measurement system with temperature effects compensation for impedance-based structural health monitoring". *Structural Health Monitoring*, Vol. 11, No. 2, pp. 173–186.

Bhalla, S. and Soh, C.K., 2004. "Electromechanical impedance modeling for adhesively bonded piezo-transducers". *Journal of Intelligent Material Systems and Structures*, Vol. 15, No. 12, pp. 955–972.

Campeiro, L.M., da Silveira, R.Z.M. and Baptista, F.G., 2018. "Impedance-based damage detection under noise and vibration effects". *Structural Health Monitoring*, Vol. 17, No. 3, p. 654–667.

Divsholi, B.S. and Yang, Y., 2012. "Health monitoring of steel structures using sub-frequency electromechanical impedance technique". *Journal of Nondestructive Evaluation*, Vol. 31, p. 197–207.

Farrar, C.R., Lieven, N.A.J. and Bement, M.T., 2005. *Damage Prognosis for Aerospace, Civil and Mechanical Systems*. Wiley, 1st edition.

Gebhart, B., 1969. *Applied Mechanics Reviews*, Vol. 22, No 7. American Society of Mechanical Engineers.

Gomes, G.F. and Giovani, R.S., 2022. "An efficient two-step damage identification method using sunflower optimization algorithm and mode shape curvature (msdbi–sfo)". *Engineering with Computers*, Vol. 38, p. 1711–1730.

Gonçalves, P.J.P., Peplow, A. and Brennan, M.J., 2018. "Exact expressions for numerical evaluation of high order modes of vibration in uniform euler-bernoulli beams". *Applied Acoustics*, Vol. 141, pp. 371–373.

Gonçalves, P., Brennan, M. and Elliott, S., 2007. "Numerical evaluation of high-order modes of vibration in uniform euler–bernoulli beams". *Journal of Sound and Vibration*, Vol. 301, No. 3, pp. 1035–1039.

Gyuhae Park, Hoon Sohn, C.R.F. and Inman, D.J., 2003. "Overview of piezoelectric impedance-based health monitoring and path forward". *The Shock and Vibration Digest*, Vol. 35, No. 6, pp. 451–463.

Hall, J.F., 2006. "Problems encountered from the use (or misuse) of rayleigh damping". *Earthquake Engineering & Structural Dynamics*, Vol. 35, No. 5, pp. 525–545.

Hamzeloo, S.R., Barzegar, M. and Mohsenzadeh, M., 2020. "Damage detection of l-shaped beam structure with a crack by electromechanical impedance response: Analytical approach and experimental validation". *Journal of Nondestructive Evaluation*, Vol. 39, No. 47.

Han, Q., Ma, Q. and andMing Liu, J.X., 2021. "Structural health monitoring research under varying temperature condition:

a review". *Journal of Civil Structural Health Monitoring*, Vol. 11, p. 149–173.

Liang, C., Sun, F.P. and Rogers, C.A., 1993. "Coupled electromechanical analysis of piezoelectric ceramic actuator-driven systems: determination of the actuator power consumption and system energy transfer". *Smart Structures and Materials*.

Liu, M. and Gorman, D., 1995. "Formulation of rayleigh damping and its extensions". *Computers & Structures*, Vol. 57, No. 2, pp. 277–285.

Luo, Z., Cao, H., Meng, L. and Lin, L., 2013. "Influences of mechanical contact on damage evaluation with electromechanical impedance technique". *Journal of Intelligent Material Systems and Structures*, Vol. 25, No. 3, p. 321–331.

Meseguer, V.J.L., Martínez-Conesa, E.J. and Portolés, A., 2019. "Numerical-experimental validation of the welding thermal cycle carried out with the mig welding process on a 6063-t5 aluminum tubular profile". *Thermal Science*, Vol. 23, No. 6A, pp. 3639–3650.

Na, W.S. and Baek, J., 2018. "A review of the piezoelectric electromechanical impedance based structural health monitoring technique for engineering structures". *Sensors*, Vol. 18, No. 5.

Selva, P., Cherrier, O., Budinger, V., Lachaud, F. and Morlier, J., 2013. "Smart monitoring of aeronautical composites plates based on electromechanical impedance measurements and artificial neural networks". *Engineering Structures*, Vol. 56, pp. 794–804.

Sepehry, N., Bakhtiari-Nejad, F. and Shamshirsaz, M., 2014. "Thermo-electro-mechanical impedance based structural health monitoring of plates". *Composite Structures*, Vol. 116, pp. 147–164.

Sepehry, N., Bakhtiari-Nejad, F. and Shamshirsaz, M., 2017. "Discrete singular convolution and spectral finite element method for predicting electromechanical impedance applied on rectangular plates". *Journal of Intelligent Material Systems and Structures*, Vol. 28, No. 18, p. 2473–2488.

Sepehry, N., Shamshirsaz, M. and Bastani, A., 2010. "Experimental and theoretical analysis in impedance-based structural health monitoring with varying temperature". *Structural Health Monitoring*, Vol. 10, No. 6, pp. 573–585.

Sun, F. P., C.Z.L.C. and Rogers, C.A., 1995. "Truss structure integrity identification using pzt sensor-actuator". *Journal of Intelligent Material Systems and Structures*, Vol. 6, No. 1, pp. 134–139.

Wang, D., Song, H. and Zhu, H., 2014. "Electromechanical impedance analysis on piezoelectric smart beam with a crack based on spectral element method". *Mathematical Problems in Engineering*, p. 13.

Wang, D., Song, H. and Zhu, H., 2015. "Electromechanical impedance analysis on piezoelectric smart beam with a crack based on spectral element method". *Mathematical Problems in Engineering*, p. 13.

Worden, K. and Dulieu-Barton, J., 2004. "An overview of intelligent fault detection in systems and structures". *Structural Health Monitoring*, Vol. 3, No. 1, p. 85–98.

Xu, G., Xu, B., Xu, C. and Luo, Y., 2016. "Temperature effects in the analysis of electromechanical impedance by using spectral element method". *Multidiscipline Modeling in Materials and Structures*, Vol. 12, No. 1, pp. 119–132.

Yan, W., Wang, J., Chen, W. and Li, W., 2011. "Electromechanical impedance response of a cracked functionally graded beam with imperfectly bonded piezoelectric wafers". *Journal of Intelligent Material Systems and Structures*, Vol. 22, No. 16, pp. 1899–1912.

Yang, Y., Lim, Y.Y. and Soh, C.K., 2008. "Practical issues related to the application of the electromechanical impedance technique in the structural health monitoring of civil structures: I. experiment". *Smart Materials and Structures*, Vol. 17, No. 3, p. 035008.

Zhang, Y., Xu, F., Chen, J., Wu, C. and Wen, D., 2011. "Electromechanical impedance response of a cracked timoshenko beam". *Sensors*, Vol. 11, No. 7, pp. 7285–7301.

7. RESPONSIBILITY NOTICE

The authors are solely responsible for the printed material included in this paper.